A Model for Dynamic Simulation and Analysis of Tether Momentum Exchange

Stephen Canfield*, David Johnson
Department of Mechanical Engineering
Tennessee Technological University
Cookeville, TN 38505

Kirk Sorensen, Ken Welzyn
TD40, TD15
NASA Marshall Space Flight Center
Huntsville AL 35812

Abstract:

Momentum-exchange/electrodynamic reboost (MXER) tether systems may enable high-energy missions to the Moon, Mars and beyond by serving as an "upper stage in space". Existing rockets that use an MXER tether station could double their capability to launch communications satellites and help improve US competitiveness. A MXER tether station would boost spacecraft from low Earth orbit to a high-energy orbit quickly, like a high-thrust rocket. Then, using the same principles that make an electric motor work, it would slowly rebuild its orbital momentum by pushing against the Earth's magnetic field--without using any propellant. One of the significant challenges in developing a momentum-exchange/electrodynamic reboost tether systems is in the analysis and design of the capture mechanism and its effects on the overall dynamics of the system. This paper will present a model for a momentum-exchange tether system that can simulate and evaluate the performance and requirements of such a system.

1. Introduction:

Many uses for space tethers have been proposed and discussed in the literature (see for example Beletsky and Levin [1], Carroll [2]). One area of proposed use is in creating an in-space payload

* Corresponding Author, Box 5014, Tennessee Technological University, Cookeville, TN 38505, (931) 372-6359, Scanfield@tntech.edu

transportation system. For example, Carroll [2] presented an early tether momentum transfer system that functioned by changing the tether length in resonance with the in-plane libration frequency to accelerate a payload. Hoyt, [3] and Forward [4] demonstrated a concept for performing momentum exchange between a spinning tether and a payload to transfer the payload into a lunar orbit, with capture and release of the payload performed at perigee of an elliptical tether orbit. Bangham, Lorenzini and Vestal [5] analyzed both single and multiple spinning-tether systems for boosting payloads from low-earth to geostationary orbits, with the multi-tether system offering the lowest mass. Hoyt et al. [6] and Hoyt [7] demonstrated a single tether system for boosting payloads from a low Earth orbit to a geostationary orbit. This system was designed to also provide transfer of payloads to lunar orbits and future transfer to the Moon and Mars. Sorenesen [8] considered the results of the Tether transporation study (Bangham, Lorenzini and Vestal [5]) and concluded that a non-equatorial, multi-tether system is nonviable due to orbital regression. Sorensen also discussed the use of electrodynamic reboost for the tether facility, described the tether/payload rendezvous, and presented a passive capture mechanism for the rendezvous process.

One important issue in the early consideration of a tether momentum-exchange facility is the dynamic behavior of the system. Several tether dynamic models have been presented in the literature, with a number of commercial or applied tether model analyses developed. Misra and Modi [9], offer a thorough review of the modeling approaches for electrodynamic tethers while continued work includes lumped-bead formulations (Keshmiri and Misra [10]) hinged-rod models (Puig-Suari et al [11], Biswell et al [12]), analytic models (Beatty and Haddow, [13]) and numerical techniques for simulating system partial differential equations (Yokota, Bekele, and Steigmann [14]). These models primarily consider single or multi-chain electrodynamic tethers during deployment, flight and retrieval from a larger vehicle. In the application of tether momentum exchange, a simulation of the nonlinear dynamic behavior of a free, spinning tether system in orbit and during the momentum exchange process is of interest and the subject

of this paper. This paper will investigate the dynamics of the momentum exchange process based on a spinning, orbiting tether facility and a passive capture mechanism as suggested by Sorensen [8]. The paper will develop a model for this tether system based on a finite element approach and perform subsequent simulation and analysis of the dynamics of the momentum exchange (MX) procedure. This approach is based in part on the techniques of finite element analysis of dynamic systems demonstrated for example by Meirovitch [15] and Nath and Ghosh [16]. The model will be general to allow a variety of tether and capture element types to be included in the future, allowing the simulation to be used as a design-guide in determining the parameters in a capture device. The model will be employed to simulate the rendezvous process with the effects on the tether system examined and considered.

2. A Model for Tether Simulation

The dynamics of a flexible tether in space flight are evaluated using a finite element model formulation of the continuous flexible tether system that will include expressions for the coriolis, tangential and normal components of elastic accelerations. The objective of this dynamic model is to observe the time response of the flexible system during tether flight and through the momentum exchange process. This finite element dynamic model will represent the tether system as a series of cable elements, each undergoing a combination of rigid body motion and axial elastic deformation and allowing free rotation between adjacent cable elements. The finite element method will be applied to this system as a means of representing the total tether motion as the motion of a continuous assembly of finite elements, with each element representing a part of the tether system, and requiring continuity and compatibility between connecting elements.

2.1 Finite Element Model

The finite element approach provides an approximate means to express the displacement of any point within a continuous element in terms of the displacement of a finite number of nodes multiplied by a

suitable set of interpolation functions (Meirovitch [15]). The interpolation functions are typically selected as a polynomial of order n, generally of low-degree, and are the same for all elements of a given type. Use of these interpolation functions to describe element motion can then result in approximate solutions for the governing partial differential equations for each element.

Consider the case of a single tether element in an equatorial orbit around the earth, shown in Fig. 1. This element represents a small portion of the entire tether system divided into a series of similar elements. The equations of motion will be derived for this representative tether element using the finite element method approximations and Lagrange's equations, and will provide the basis to assemble a system of similar elements and thus a complete tether system.

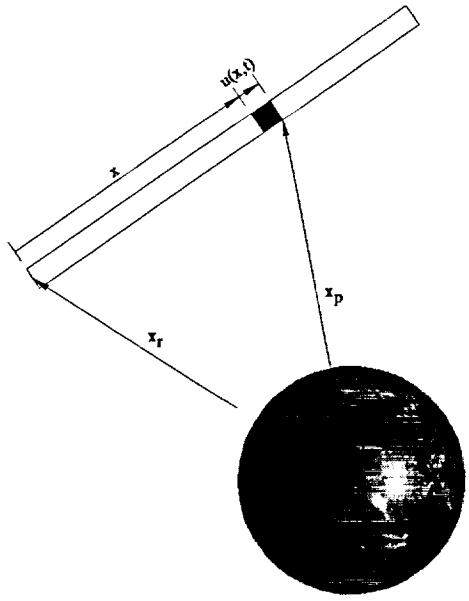

Figure 1: Tether element in equatorial Earth orbit

The location of particle dx on the tether element shown in fig. 1 is given by $\mathbf{x}_p$ as:

$$\mathbf{x}_p(x,t) = \mathbf{x}_r(t) + \mathbf{R}_{elem}(x + u(x,t)) \qquad \text{Eq. 1}$$

with $u(x,t)$ representing the elastic axial displacement of the element at point x along the element in time, both described in the element frame, and $\mathbf{R}_{elem}$ a suitable rotation operator expressing the displacements in a uniform frame. Using the selected interpolation functions, the axial displacement can be written as

$$u(x,t) = \mathbf{l}(x)^T \mathbf{u}(t) \qquad \text{Eq. 2}$$

with $\mathbf{l}(x)^T = [L_1(x) \quad L_2(x) \quad \ldots]^T$ the interpolation functions and $\mathbf{u}(t) = [u_1(t) \quad u_2(t) \quad \ldots]^T$ the nodal displacements in time. The particle position can be defined as a combination of these interpolation functions and nodal positions as,

$$\mathbf{x}_p(x,t) = \mathbf{x}_r(t) + \mathbf{R}_{elem}\left(x + \mathbf{l}(x)^T \mathbf{u}(t)\right). \qquad \text{Eq. 3}$$

A set of generalized coordinates will be defined to describe the motion of the tether element. This set will consist of the reference position, $\mathbf{x}_r$, the orientation of the element defined in a rotation operator, $\mathbf{R}$, and the nodal displacements, $\mathbf{u}$. This vector of generalized coordinates, $\mathbf{q}$, becomes

$$\mathbf{q} = \mathbf{R}\boldsymbol{\mu} \qquad \text{Eq. 4}$$

with $\mathbf{R}$ containing element rotation and $\boldsymbol{\mu}$ defined as

$$\boldsymbol{\mu} = \begin{bmatrix} x_{rx} & x_{ry} & 1 & u_1 & u_2 \end{bmatrix}^T. \qquad \text{Eq. 5}$$

The position of any point along the element is then given as a combination of the interpolation functions, cast into matrix form, $\mathbf{L}^T$ and the generalized coordinates,

$$\mathbf{x}_p = \mathbf{L}^T \mathbf{R}\boldsymbol{\mu}. \qquad \text{Eq. 6}$$

Note that $\mathbf{L}^T$ contains the spatial dependencies along the tether length while $\mathbf{R}$ and $\boldsymbol{\mu}$ are functions of time. To proceed with Lagrange's equations, the Lagrangian must be formed as the combination of kinetic energy and potential energy in the tether element. The kinetic energy is first defined over the element,

$$T = \frac{1}{2}\int_0^l \rho(x)A(x)\left(\frac{\partial \mathbf{x}_p}{\partial t}\right)^2 dx = \frac{1}{2}\int_0^l \rho(x)A(x)\left(\frac{\partial\left(\mathbf{L}^T\mathbf{R}\boldsymbol{\mu}\right)}{\partial t}\right)^2 dx \qquad \text{Eq. 7}$$

with l the tether element length $A(x)$ the element cross section area and $\rho(x)$ the element density. The velocity of the tether element at location x is

$$\dot{\mathbf{x}}_p = \mathbf{L}^T\mathbf{R}\dot{\boldsymbol{\mu}} + \mathbf{L}^T\dot{\mathbf{R}}\boldsymbol{\mu} \qquad \text{Eq. 8}$$

with $\dot{\mathbf{R}}$ providing the angular velocity of the tether element frame. This will be recast to combine the generalized coordinate velocities into a single vector, $\dot{\boldsymbol{\mu}}'$ as

$$\dot{\mathbf{x}}_p = \mathbf{L}^T\mathbf{R}'\dot{\boldsymbol{\mu}}' \qquad \text{Eq. 9}$$

where $\mathbf{R}'$ is a general operator that gives velocity orientation.

This paper will consider tether motion in an equatorial plane. Figure 2 shows the generalized coordinates for this planar case, in which $\dot{\boldsymbol{\mu}}'$, $\mathbf{L}^T$ and $\mathbf{R}'$ for element 1 become

$$\dot{\boldsymbol{\mu}}' = \begin{bmatrix} \dot{x}_{rx} & \dot{x}_{ry} & \dot{\theta} & \dot{\theta}u_1 & \dot{\theta}u_2 & \dot{u}_1 & \dot{u}_2 \end{bmatrix}^T \qquad \text{Eq. 10}$$

$$\mathbf{L}^T = \begin{bmatrix} 1 & 0 & x & 0 & L_1 & 0 & L_2 & 0 \\ 0 & 1 & 0 & x & 0 & L_1 & 0 & L_2 \end{bmatrix}, \mathbf{R}' = \begin{bmatrix} 1 & 0 & 0 & 0 & 0 & 0 & 0 \\ 0 & 1 & 0 & 0 & 0 & 0 & 0 \\ 0 & 0 & s\theta & 0 & 0 & 0 & 0 \\ 0 & 0 & c\theta & 0 & 0 & 0 & 0 \\ 0 & 0 & 0 & -s\theta & 0 & c\theta & 0 \\ 0 & 0 & 0 & c\theta & 0 & s\theta & 0 \\ 0 & 0 & 0 & 0 & -s\theta & 0 & c\theta \\ 0 & 0 & 0 & 0 & c\theta & 0 & s\theta \end{bmatrix} \qquad \text{Eq. 11}$$

with $L_1 = \frac{1-x}{l}$, $L_2 = \frac{x}{l}$ defining a linear set of interpolation functions.

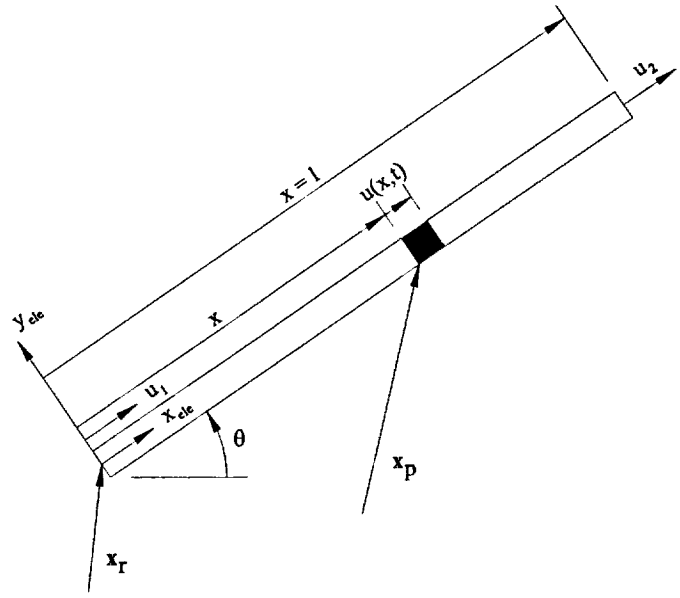

Figure 2: Generalized coordinates of a tether element

Using the expression of $\dot{\mathbf{x}}_p$ given in Eq. 9, the kinetic energy can be rewritten as,

$$T = \frac{1}{2}\int_0^l \rho(x)A(x)\left(\mathbf{L}^T\mathbf{R}'\dot{\boldsymbol{\mu}}'\right)^2 dx = \frac{1}{2}\dot{\boldsymbol{\mu}}'^T\,\mathbf{R}'^T\left[\int_0^l \rho(x)A(x)\mathbf{L}\mathbf{L}^T dx\right]\mathbf{R}'\dot{\boldsymbol{\mu}}' \qquad \text{Eq. 12}$$

or

$$T = \frac{1}{2}\dot{\boldsymbol{\mu}}'^T\,\mathbf{R}'^T\,\mathbf{m}_e\mathbf{R}'\dot{\boldsymbol{\mu}}' \qquad \text{Eq. 13}$$

with $\mathbf{m}_e$ the consistent element mass matrix determined from the interpolation matrix and element area and density as

$$\mathbf{m}_e = \int_0^l \rho(x)A(x)\mathbf{L}\mathbf{L}^T dx\,. \qquad \text{Eq. 14}$$

This element mass matrix $\mathbf{m}_e$ is shown for reference in the appendix. In a manner similar to evaluating the kinetic energy, the potential energy of the tether element is evaluated. In this derivation, the potential energy will consider strain energy in the element only, while gravitational potential along with other external loads will be included in the generalized force. The potential energy in the element is given as

$$V = \frac{1}{2}\int_0^l AE(x)\left(\frac{\partial \mathbf{x}_p}{\partial x}\right)^2 dx. \qquad \text{Eq. 15}$$

Using the expression for $\mathbf{x}_p$ given in Eq. 6,

$$V = \frac{1}{2}\int_0^l AE(x)\left(\frac{\partial \mathbf{L}^T\mathbf{R}\boldsymbol{\mu}}{\partial x}\right)^2 dx = \frac{1}{2}\boldsymbol{\mu}^T\mathbf{R}^T\mathbf{k}_e\mathbf{R}\boldsymbol{\mu} \qquad \text{Eq. 16}$$

with A and E the element area and modulus, and $\mathbf{k}_e$ the element stiffness matrix evaluated as,

$$\mathbf{k}_e = \int_0^l AE(x)\frac{\partial \mathbf{L}}{\partial x}\frac{\partial \mathbf{L}^T}{\partial x}dx. \qquad \text{Eq. 17}$$

The element stiffness matrix $\mathbf{k}_e$ is given for reference in the appendix. The generalized force is constructed next to represent external forces located at the nodes. This is derived from an expression of the virtual work resulting from the gravitational loads and all nonconservative forces distributed over the element,

$$\delta W = \int_0^l \mathbf{f}(x,t)\cdot\delta\mathbf{x}_p dx = \int_0^l \mathbf{f}(x,t)\cdot\mathbf{L}^T\delta(\mathbf{R}\boldsymbol{\mu})dx = \mathbf{F}\delta(\mathbf{R}\boldsymbol{\mu}) \qquad \text{Eq. 18}$$

with $\mathbf{f}(x,t)$ the external force distribution over the element and $\mathbf{F}$ the external nodal force given as:

$$\mathbf{F}_e = \int_0^l \mathbf{f}(x,t)\cdot\mathbf{L}^T dx. \qquad \text{Eq. 19}$$

Partial derivatives of the Lagrangian, $\Im = T - V$, with respect to the generalized coordinates and their time derivatives are evaluated next. In general form, the elements of Lagrange's equations are considered as,

$$\partial\Im/\partial\dot{q}_i = \partial T/\partial\dot{q}_i - \partial V/\partial\dot{q}_i = \partial\dot{\boldsymbol{\mu}}'^T/\partial\dot{q}_i\,\mathbf{R}'^T\mathbf{m}_e\mathbf{R}'\boldsymbol{\mu}' \qquad \text{Eq. 20}$$

$$\frac{d}{dt}\left(\partial\Im/\partial\dot{q}_i\right) = \frac{d}{dt}\left(\partial\dot{\boldsymbol{\mu}}'^T/\partial\dot{q}_i\,\mathbf{R}'^T\mathbf{m}_e\mathbf{R}'\boldsymbol{\mu}'\right) = \frac{d}{dt}\left(\partial\dot{\boldsymbol{\mu}}'^T/\partial\dot{q}_i\right)\mathbf{R}'^T\mathbf{m}_e\mathbf{R}'\boldsymbol{\mu}' + 2\,\partial\dot{\boldsymbol{\mu}}'^T/\partial\dot{q}_i\,\dot{\mathbf{R}}'^T\mathbf{m}_e\mathbf{R}'\boldsymbol{\mu}' + \partial\dot{\boldsymbol{\mu}}'^T/\partial\dot{q}_i\,\mathbf{R}'^T\mathbf{m}_e\mathbf{R}'\ddot{\boldsymbol{\mu}}' \qquad \text{Eq. 21}$$

$$\partial\Im/\partial q_i = \partial T/\partial q_i - \partial V/\partial q_i = \partial\dot{\boldsymbol{\mu}}'^T/\partial q_i\,\mathbf{R}'^T\mathbf{m}_e\mathbf{R}'\dot{\boldsymbol{\mu}}'+\dot{\boldsymbol{\mu}}'^T\,\partial\mathbf{R}'^T/\partial q_i\,\mathbf{m}_e\mathbf{R}'\dot{\boldsymbol{\mu}}'-\partial\boldsymbol{\mu}^T/\partial q_i\,\mathbf{R}^T\mathbf{k}_e\mathbf{R}\boldsymbol{\mu}-\boldsymbol{\mu}^T\,\partial\mathbf{R}^T/\partial q_i\,\mathbf{k}_e\mathbf{R}\boldsymbol{\mu} \quad \text{Eq. 22}$$

and the generalized force associated with q_i is derived from the virtual work as,

$$Q_i = \mathbf{F}_e\cdot\left(\mathbf{R}\,\partial\boldsymbol{\mu}/\partial q_i + \partial\mathbf{R}/\partial q_i\,\boldsymbol{\mu}\right). \quad \text{Eq. 23}$$

From these partial and time derivatives, the equations of motion for the element are assembled for each generalized coordinate, i,

$$\frac{d}{dt}\left(\partial\Im/\partial\dot{q}_i\right)-\partial\Im/\partial\dot{q}_i = Q_i \quad \text{Eq. 24}$$

$$\begin{aligned}\frac{d}{dt}\left(\partial\dot{\boldsymbol{\mu}}'^T/\partial\dot{q}_i\right)\mathbf{R}'^T\mathbf{m}_e\mathbf{R}'\dot{\boldsymbol{\mu}}'+2\,\partial\dot{\boldsymbol{\mu}}'^T/\partial\dot{q}_i\,\dot{\mathbf{R}}'^T\mathbf{m}_e\mathbf{R}'\dot{\boldsymbol{\mu}}'+\partial\dot{\boldsymbol{\mu}}'^T/\partial\dot{q}_i\,\mathbf{R}'^T\mathbf{m}_e\mathbf{R}'\ddot{\boldsymbol{\mu}}'\\ -\partial\dot{\boldsymbol{\mu}}'^T/\partial q_i\,\mathbf{R}'^T\mathbf{m}_e\mathbf{R}'\dot{\boldsymbol{\mu}}'-\dot{\boldsymbol{\mu}}'^T\,\partial\mathbf{R}'^T/\partial q_i\,\mathbf{m}_e\mathbf{R}'\dot{\boldsymbol{\mu}}'+\partial\boldsymbol{\mu}^T/\partial q_i\,\mathbf{R}^T\mathbf{k}_e\mathbf{R}\boldsymbol{\mu}+\boldsymbol{\mu}^T\,\partial\mathbf{R}^T/\partial q_i\,\mathbf{k}_e\mathbf{R}\boldsymbol{\mu}=Q_i\end{aligned} \quad \text{Eq. 25}$$

for i =1 … m, to result in m equations of motion with m the number of generalized coordinates.

After expanding the system of equations in Eq. 25 for each generalized coordinate and combining accelerations, the equations of motion take on the general form

$$\mathbf{M}_e\ddot{\boldsymbol{\mu}}'+\mathbf{D}_e(q,\dot{q})\dot{\boldsymbol{\mu}}'+\mathbf{K}_e(q)\boldsymbol{\mu}=\mathbf{Q}_e \quad \text{Eq. 26}$$

with

$$\mathbf{M}_e=\begin{bmatrix}\partial\dot{\boldsymbol{\mu}}'^T/\partial\dot{q}_1\\ \partial\dot{\boldsymbol{\mu}}'^T/\partial\dot{q}_2\\ \vdots\\ \partial\dot{\boldsymbol{\mu}}'^T/\partial\dot{q}_m\end{bmatrix}\mathbf{R}'^T\mathbf{m}_e\mathbf{R}' \quad \text{Eq. 27}$$

$$\mathbf{D}_e(q,\dot{q}) = \left(\begin{bmatrix} \frac{d}{dt}\left(\partial\dot{\boldsymbol{\mu}}'^T/\partial\dot{q}_1\right) - \partial\dot{\boldsymbol{\mu}}'^T/\partial q_1 \\ \frac{d}{dt}\left(\partial\dot{\boldsymbol{\mu}}'^T/\partial\dot{q}_2\right) - \partial\dot{\boldsymbol{\mu}}'^T/\partial q_2 \\ \vdots \\ \frac{d}{dt}\left(\partial\dot{\boldsymbol{\mu}}'^T/\partial\dot{q}_m\right) - \partial\dot{\boldsymbol{\mu}}'^T/\partial q_m \end{bmatrix} \mathbf{R}'^T + 2\begin{bmatrix} \partial\dot{\boldsymbol{\mu}}'^T/\partial\dot{q}_1 \\ \partial\dot{\boldsymbol{\mu}}'^T/\partial\dot{q}_2 \\ \vdots \\ \partial\dot{\boldsymbol{\mu}}'^T/\partial\dot{q}_m \end{bmatrix} \dot{\mathbf{R}}'^T - \begin{bmatrix} \dot{\boldsymbol{\mu}}'^T\,\partial\mathbf{R}'^T/\partial q_1 \\ \dot{\boldsymbol{\mu}}'^T\,\partial\mathbf{R}'^T/\partial q_2 \\ \vdots \\ \dot{\boldsymbol{\mu}}'^T\,\partial\mathbf{R}'^T/\partial q_m \end{bmatrix} \right) \mathbf{m}_e\mathbf{R}' \quad \text{Eq. 28}$$

$$\mathbf{K}_e(q) = \left(\begin{bmatrix} \partial\boldsymbol{\mu}^T/\partial q_1 \\ \partial\boldsymbol{\mu}^T/\partial q_2 \\ \vdots \\ \partial\boldsymbol{\mu}^T/\partial q_m \end{bmatrix} \mathbf{R}^T + \begin{bmatrix} \boldsymbol{\mu}^T\,\partial\mathbf{R}^T/\partial q_1 \\ \boldsymbol{\mu}^T\,\partial\mathbf{R}^T/\partial q_2 \\ \vdots \\ \boldsymbol{\mu}^T\,\partial\mathbf{R}^T/\partial q_m \end{bmatrix} \right) \mathbf{k}_e\mathbf{R} \quad \text{Eq. 29}$$

$$\mathbf{Q}_e = \begin{bmatrix} \mathbf{F}_e\left(\mathbf{R}\,\partial\boldsymbol{\mu}/\partial q_1 + \partial\mathbf{R}/\partial q_1\,\boldsymbol{\mu}\right) \\ \mathbf{F}_e\left(\mathbf{R}\,\partial\boldsymbol{\mu}/\partial q_2 + \partial\mathbf{R}/\partial q_2\,\boldsymbol{\mu}\right) \\ \vdots \\ \mathbf{F}_e\left(\mathbf{R}\,\partial\boldsymbol{\mu}/\partial q_n + \partial\mathbf{R}/\partial q_n\,\boldsymbol{\mu}\right) \end{bmatrix}. \quad \text{Eq. 30}$$

An expansion of each of these terms is listed in the appendix. Thus, Eq. 26 provides the equations of motion for the tether element of Fig. 2. It now remains to perform an assembly process by which the equations for all the elements forming the tether system are compiled.

2.2 Element Assembly:

The assembly procedure allows the entire tether system to be represented as a collection of elements, with geometric compatibility maintained at all element nodes. Let fig. 3 represent a portion of the tether system modeled as a collection of tether elements.

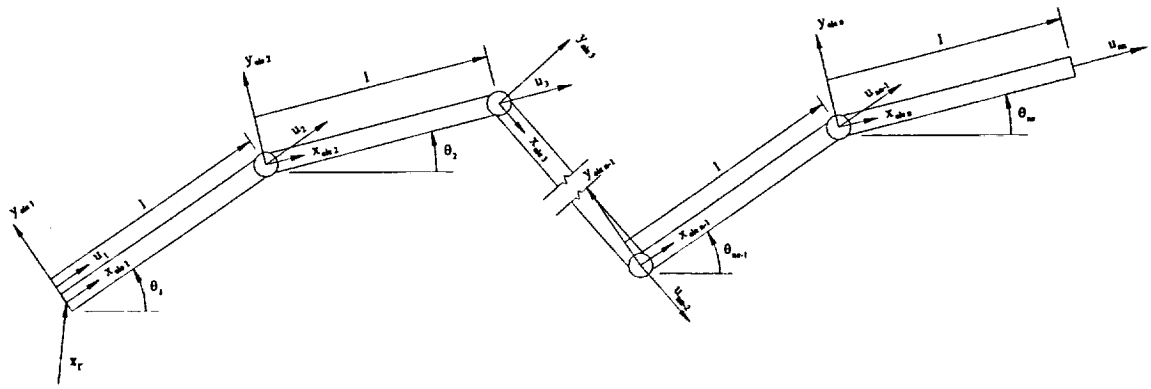

Figure 3: Collection of elements forming the tether system

Each element is attached to the end node of the previous element and maintains continuity through nodal displacement. As additional elements are added to the tether system, additional generalized coordinates appear. For example, in this case of a planar tether system, two new generalized coordinates occur with each additional element. Thus, the vector of generalized coordinates for a tether with n elements is,

$$\mathbf{q} = \begin{bmatrix} x_{rx} & x_{ry} & \theta_1 & u_1 & u_2 & \theta_2 & \cdots & \theta_n & u_{n+1} \end{bmatrix}^T. \qquad \text{Eq. 31}$$

For a system with n elements, there are $m = 3+2n$ generalized coordinates.

The equations of motion for the entire tether system are constructed through assembly of the individual element equations of motion, while taking into account continuity at the nodal positions. The assembly procedure can be observed by forming the total kinetic and potential energy and virtual work of the tether system as a sum of the energies and virtual work contributed by each element.

$$T_{tether} = \frac{1}{2}\sum_{i=1}^{n} \dot{\boldsymbol{\mu}}'^{T}_{i}\, \mathbf{R}'^{T}_{i}\, \mathbf{m}_{ei} \mathbf{R}'_{i}\, \dot{\boldsymbol{\mu}}'_{i},$$

$$V_{tether} = \frac{1}{2}\sum_{i=1}^{n} \int_0^l A_i E_i(x) \left(\frac{\partial \mathbf{L}^T \mathbf{R}_i \boldsymbol{\mu}_i}{\partial x} \right)^2 dx \qquad \text{Eq. 32}$$

$$\delta W_{tether} = \sum_{i=1}^{n} \int_0^l \mathbf{f}_i(x,t) \cdot \mathbf{L}^{\mathrm{T}} \delta(\mathbf{R}_i \boldsymbol{\mu}_i) dx$$

which leads to Lagrange's equations for the system,

$$\Im_{tether} = T_{tether} - V_{tether}, \quad \partial \Im_{tether} / \partial \dot{q}_k = \sum_{i=1}^{n} \left(\partial T / \partial \dot{q}_k - \partial V / \partial \dot{q}_k \right), \text{ etc.} \qquad \text{Eq. 33}$$

To make the individual elements compatible in the summation processes, a uniform set of descriptive coordinates must be developed for each element, similar to Eq. 6 for the first element. Consider an internal element, call it the i^{th} element, located along the tether (refer for example to Fig. 3). The position of a point along the i^{th} tether can then be given using the same form as equation 6,

$$\mathbf{x}_{pi} = \mathbf{L}^T \mathbf{R}_i \boldsymbol{\mu}_i \qquad \text{Eq. 34}$$

with the displacement vector, μ_i given as:

$$\boldsymbol{\mu}_i = \left[x_{rx} + \sum_{j=1}^{i-1} \cos(\theta_j)(l_j + u_{j+1}) \quad x_{ry} + \sum_{j=1}^{i-1} \sin(\theta_j)(l_j + u_{j+1}) \quad 1 \quad u_i \quad u_{i+1} \right]^T \qquad \text{Eq. 35}$$

and $\mathbf{R}_i$ the rotation operator for element i. Thus, the position of a point on the i^{th} tether element is a function of the tether reference vector as well as all preceding nodal displacements and element orientations. In a similar manner, the velocity of a point on the i^{th} tether element is generalized to become,

$$\dot{\mathbf{x}}_{pi} = \mathbf{L}^{\mathrm{T}} \mathbf{R}'_i\, \dot{\boldsymbol{\mu}}'_i \qquad \text{Eq. 36}$$

with $\mathbf{R}'_i$ a general operator that gives velocity orientation for element i and

$$\dot{\boldsymbol{\mu}}'_i = \left[\dot{x}_{rx} + \sum_{j=1}^{i-1} \left[-\dot{\theta}_j \sin(\theta_j)(l_j + u_{j+1}) + \cos(\theta_j)\dot{u}_{j+1} \right] \quad \dot{x}_{ry} + \sum_{j=1}^{i-1} \left[\dot{\theta}_j \cos(\theta_j)(l_j + u_{j+1}) + \sin(\theta_j)\dot{u}_{j+1} \right] \quad \dot{\theta}_i \quad \dot{\theta}_i u_i \quad \dot{\theta}_i u_{i+1} \quad \dot{u}_i \quad \dot{u}_{i+1} \right]^T \qquad \text{Eq. 37}$$

Using these general expressions for the position and velocity of reference positions for each element, the equations of motion can be derived for the entire system through the summation process demonstrated above, resulting in a general form for the equations of motion for the entire tether system,

$$\mathbf{M}\ddot{\mathbf{q}} + \mathbf{D}(q, \dot{q})\dot{\mathbf{q}} + \mathbf{K}(q)\mathbf{q} = \mathbf{Q} \qquad \text{Eq. 38}$$

where $\ddot{\mathbf{q}}$, $\dot{\mathbf{q}}$ and $\mathbf{q}$ represent the generalized coordinates associated with the entire tether system, and given in the general vector form as, $\mathbf{q} = \begin{bmatrix} x_{rx} & x_{ry} & \theta_1 & u_1 & u_2 & \theta_2 & u_3 & \cdots \end{bmatrix}^T$ and the matrices, **M**, **D**, and **K** and vector **Q** are coefficients of the generalized coordinates and their derivatives. These are found in general through expanding the elements of Lagrange's equations for each element, shown for example for element 1 in Eqs. 20-23, and then combining terms to result in the necessary coefficient matrices of the generalized coordinates. The procedure is demonstrated in the appendix, with the **M**, **D**, and **K** matrices and the vector **Q** expanded for a two element system. Note that since element rotation is decoupled from the stiffness in the case of geometric linearity, the θ associated terms in the generalized vector multiplied by the stiffness matrix will be set to zero. With the general equation of motion generated for the tether system, a solution approach used in tether simulation is presented next.

2.3 Solution of Equations of Motions

Eq. 38 provides a system of second order differential equations of motion of the tether system defining the response of the generalized coordinates in time. Combining the shape functions and the nodal displacements in time, the approximated response of the continuous tether system is observed. This behavior of the rotating tether system in orbit is the point of interest in this work, and is solved using a direct integration routine. A Runge-Kutta integration procedure with adaptive time step is selected and employed for dynamic tether analysis.

2.4 Element types used in the Tether MX model

2.4.1 Tether Element:

An element with a single longitudinal non-rigid-body degree-of-freedom is first employed in the planar tether model. Elemental longitudinal stiffness and damping are associated with this non-rigid-body degree-of-freedom. Each tether element is modeled with two nodes representing a linear shape function. Rigid body motions of the tether element include rotation and translations in the orbital plane. Due to the inability of the tether element to support compressive loads, a significant nonlinearity occurs when the tether goes slack. Several models have been proposed to accommodate this nonlinearity, the simplest approach is employed in this model by defining the element stiffness to go to zero when the element goes slack,

$$\mathbf{k}_{ei} = \begin{cases} \mathbf{k}_{ei}, & l_i \geq l_{elm} \\ \mathbf{0}, & l_i \leq l_{elm} \end{cases} \qquad \text{Eq. 39}$$

Note that in the spinning tether configuration, the tether elements maintain positive tension at all times due to centripetal acceleration forces and slack conditions are generally identified as unstable conditions in the tether model.

2.4.2 Ballast and Capture Element:

The ballast or facility element represents a rigid body, ballast mass located at one end of the tether. This element will be composed of an infinitesimally small member with mass localized at a common node. Note that since the length approached zero, the stiffness approaches infinity, this is represented in the global matrix with a single node. The mass of this element is also associated with a single node, and the force effects of this element are derived for the single nodal position.

2.4 Tether Momentum Exchange

Momentum exchange occurs through the process of capture, carry and release of the payload. Initial capture of the payload is modeled as an inelastic impact process between the last node of the capture element and a rigid lumped-mass payload. The rendezvous process is included in the tether model in the following manner. The tether model is simulated through integration forward in time starting from a set of initial conditions to result in a future rendezvous with the payload. At the point of rendezvous, time t_r, algebraic evaluation of the new velocities due to impact between the point mass payload and the mass localized at the end of the tether is performed. This results in a new set of boundary and state conditions that are used to update the tether model and continue the time integration of the tether model. Payload release involves again an instantaneous change in the boundary conditions of the tether model. Note that in general, the rendezvous process is considered to occur with the end of the capture device and the payload having the same position and velocity, resulting in no net effect from impact. Error in either position or velocity of the tether or payload would add additional dynamic effects to the system.

The remainder of this paper reports on some of the results from the simulation of the momentum exchange process.

3.0 Analysis of Tether Capture and Release of Payload:

Using a simple FEA tether model, the capture process is simulated as follows. The tether simulation is started and proceeds for a period of time sufficient to allow initial condition transients to die out. Similarly, the payload is released and propagated in time in its proper orbit. Initial conditions of both the tether and payload are selected to result in a rendezvous precise in space and time. The momentum process begins when the payload enters the capture region of the tether and continues through the carry and release process. For the general case, the capture occurs when the tether is at perigee and the tether is aligned with the local vertical, the capture end pointing toward earth. The tether than carries the payload through a predetermined angle and releases the payload, with both the payload and tether assuming a new

trajectory. The simulation process records the data from the tether model including tether tension, rotation rate, center of mass, and velocity. These results provide essential information in predicting momentum exchange performance under ideal conditions, setting the bounds on required tether propagation accuracy, and in providing design guidelines for design of the capture device. Results from analysis in each of these areas follow. These results are based on tether and payload sizes published by Hoyt [7], as shown in Table I.

Table I: Tether and Payload Parameters

Constants		**Tether Facility Orbit**	
μ	3.986E+14	Perigee (m)	6,785,136.00
Payload Mass (kg)	1000, 2500	Apogee (m)	14,823,136.00
Capture Mass (kg)	250	Time for one orbit (s)	11,176.25
Ballast Mass (kg)	11000	SMA	10,804,136.00
Tether Length (m)	80000	e	0.371987172
Cross Sect Area (m^2)	1.9635E-05	Perigee Velocity (m/s)	8977.690593
ρ (kg/m^3)	970	Apogee Velocity (m/s)	4109.444293
Payload orbit		ω of tether fac. (rad/s)	-0.013881192
Orbit Radius (m)	6694275.739		
Vp (m/s)	7716.44186		
Time for one orbit (s)	5450.876936		

3.1 Results From Tether Momentum Exchange Simulation

The momentum exchange analysis will demonstrate simulation of tether and payload rendezvous, capture, carry and release, under ideal conditions. Here, ideal conditions imply that there is no error in position or velocity of either the tether or payload. At the point of rendezvous, both the capture device and payload have the same position and velocity. The tether produces and instantaneous application of acceleration on the payload in the direction of the tether, resulting in increase in tether tension with much smaller effects on transverse vibrations. The results from this ideal capture are shown in figs. 4-8. Figures 4-6 show the tether orbit radius before and after rendezvous, with Figs. 5,6 zoomed to show effects of capture and release. Figure 7 shows the payload orbit before and after rendezvous while fig. 8 gives a time history of the tether tension. Finally, Table II below summarizes the results of the orbits of

the tether facility and payload before and after the momentum exchange process. Table II shows the results for both a 1000 kg and a 2500 kg payload.

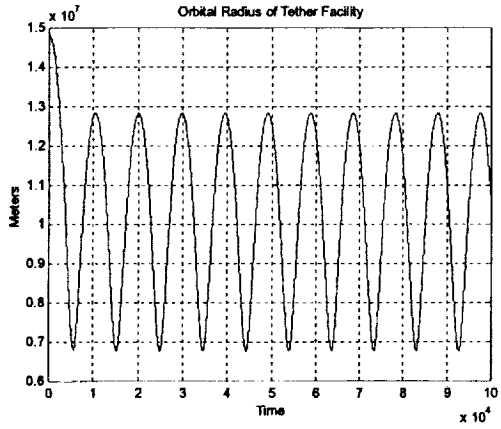

Fig. 4: Orbit Radius of Tether

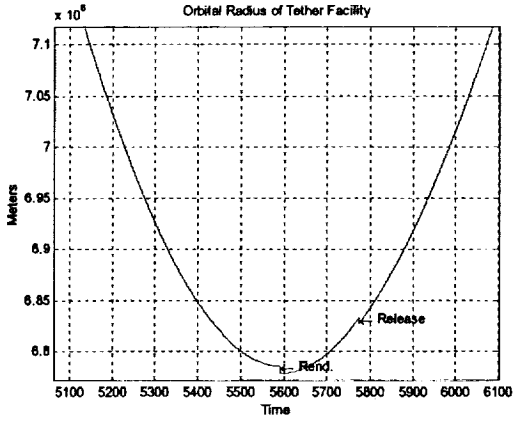

Fig. 5: Orbit Radius of Tether

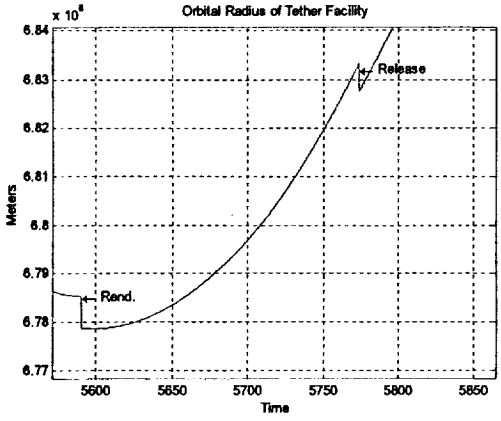

Fig. 6: Orbit Radius of Tether

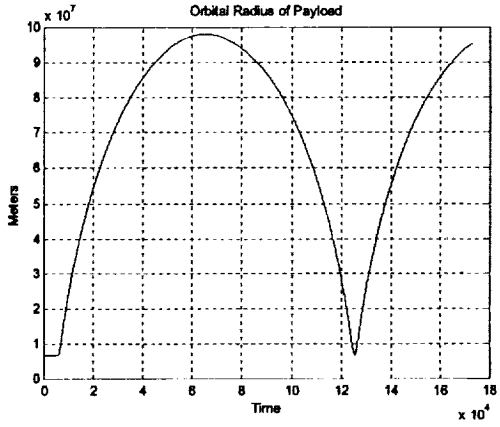

Fig. 7: Orbit Radius of Payload

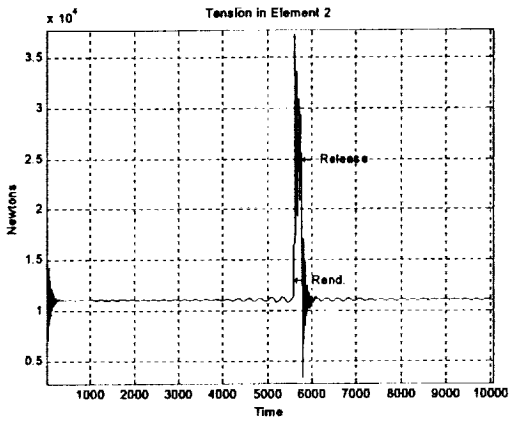

Fig. 8: Tension in Tether elements

Table II: Summary of Tether and Payload Orbits

	Payload		Tether Facility (1000 kg Payload)		Tether Facility (2500 kg Payload)	
	Pre Catch	Post Release	Pre Catch	Post Release	Pre Catch	Post Release
Perigee	6693863	6789026	6785077	6766417	6785077	6763012
Perigee Altitude	315727	410890	406941	388281	406941	384876
Apogee	6693863	97999789	14823136	12830894	14823136	11037967
Apogee Altitude	315727	91621653	8445000	6452758	8445000	4659831
Period	5450	119354	11176	9653	11176	8357
Semi-major Axis	6693863	52394407	10804106	9798655	10804106	8900490
eccentricity	0	0.8704	0.3720	0.3095	0.3720	0.2402
Perigee Velocity	7717	10479	8978	8783	8978	8549
Apogee Velocity	7717	726	4109	4632	4109	5238
ω (deg)			0	2.75	0	3.63

From the error free momentum exchange case several results are noted. First, general effects on the tether orbit correspond to those published in the current literature (Hoyt [7], Bangham et al [5]). However, the tether orbit is also affected by elastic material change during the capture and release process. The tension undergoes a significant increase during both capture and release. The tether tension is fairly stable before and after capture with small oscillations in amplitude due to tether rotation in the gravitational field. At rendezvous, the tether experiences a significant spike in tether tension. Release again causes a step input to the tether system, resulting in a damped transient response returning to the free-tether steady-state conditions. The response of the tether during the momentum exchange process is

largely dependent on the stiffness and damping characteristics of both the tether and capture elements. An additional effect is the resulting tether orbit. As predicted, the tether facility loses altitude, primarily at apogee. The orbit change in the tether facility for both the 1000 kg and 2500 kg payload is significant, but gives the tether sufficient opportunity to reboost for future momentum exchange. A final characteristic of the system is noted. The line of apisides of the tether is shifted at MX due a finite time between capture and release and the elastic behavior of the tether system.

4.0 Summary

The momentum exchange process has been modeled using an FEA approach, with the basic processes verified against current literature. The FEA model shown is based on the simplest single degree of freedom tether element and accounts for dynamic effects due to the rigid body motion and elastic deformation of the element. This model can be extended to multiple tether elements and allows for specification of various element types. The paper then presents an analysis of the dynamic effects of the momentum exchange process on a tether system and payload. This analysis demonstrates relative stability in the process and confirms many of the previously reported results. It also demonstrates a number of dynamic effects in the process such as longitudinal tether stretching and a shift in the line of apsides. Finally, the paper demonstrates the ability of the tether model to boost a variety of payloads given a sufficient time for reboost.

Acknowledgements

The authors express their appreciation for the technical support from Randy Baggett and John Glaese and the support of NASA/MSFC, contract numbers NAG8-1793 and NGT8-52911.

Bibliography

1) Beletsky, V.V., and E.M., Levin, 1993, *Dynamics of Space Tether Systems, Advances in the Astronautical Sciences*, Vol. 83, Univelt, Inc., San Diego CA.

2) Carroll J. A., 1986, "Tether Applications in Space Transporation," *Acta Astronautica*, Vol. 13, No. 4, pp. 165-174.

3) Hoyt, R.P., "Tether System for Exchanging Payloads Between Low Earth Orbit and the Lunar Surface," AIAA Paper 97-2794, *33rd AIAA/ASME/ASE/ASEE Joint Propulsion Conference*, Seattle, WA, 6-9, July 1997.

4) Forward, R. L., "Tether Transport from LEO to the Lunar Surface," AIAA paper 91-2322, *27th AIAA/ASME/ASE/ASEE Joint Propulsion Conference*, July 1991.

5) Bangham, M., Lorenzini, E., and Vestal, L., 1998, "Tether Transportation System Study," *NASA/TP-1998-206959.*

6) Hoyt, R.P., Forward, R.L., Nordley, G.D., and C.W. Uphoff, 1999, "Rapid Interplanetary Tether Transport Systems," *50th International Astronautical Congress*, Amsterdam, The Netherlands, Oct. 4-8, 1999, IAF-99-A.5.10.

7) Hoyt, R., 2000, "Design and Simulation of a Tether Boost Facility for LEO to GTO Transport," AIAA Paper 2000-3866, *36th AIAA/ASME/SAE/ASEE Joint Propulsion Conference & Exhibit*, Huntsville, AL, 17-19 July 2000.

8) Sorenesen, K., 2001, "Conceptual Design and Analysis of an MXER Tether Boost Station," AIAA 2001-3915.

9) Misra, A.K., and Modi, V.J., "A Survey of the Dynamcis and Control of Tethered Satellite Systems," *Advances in the Astronautical Sciences, Tethers in Space*, Vol. 62, 1986, pp. 667-719.

10) Keshmiri, M., and A.K. Misra, 1993, "A General Formulation for N-Body Tethered Satellite System Dynamics," AAS 93-700, pp. 623-644.

11) Poig-Suari, J., Longuski, J.M., and S. Tragesser, 1993, "A Three Dimensional Hinged-Rod Model for Flexible-Elastic Aerobraking Tethers," AAS 93-730, pp. 755-774.

12) Biswell, B.L., Puig-Suari, J., Longuski, J.M., and S.G. Tragesser, 1998, "Three-Dimensional Hinged-Rod Model for Elastic Aerobraking Tethers," *Journal of Guidance, Control and Dynamics*, Vol. 21, No. 2, March-April, pp. 286-295.

13) Beatty, M.F., and J.D. Haddow, 1985, "Transverse Impact of a Hyperelastic Stretched String," Journal of Applied Mechanics, Vol. 52, No. 1, pp. 137-143.

14) Yokota, J.W., Bekele, S.A., and D.J. Steigmann, 2001, "Simulation the Nonlinear Dynamics of an Elastic Cable," *AIAA Journal*, Vol. 39, No. 3, pp. 504-510

15) Meirovitch L., 1986, *Elements of Vibration Analysis,* McGraw-Hill, Boston MA.

16) Nath, P.K. and A. Ghosh, 1980, "Kineto-Elastodynamic Analysis of Mechanisms by Finite Element Method," *Mechanism and Machine Theory*, Vol. 15, pp. 179-197.

Appendix:

The general displacement of a particle along element i is given as a combination of the interpolation functions in the form,

$$\mathbf{x}_{pi} = \mathbf{L}^T \mathbf{R}_i \boldsymbol{\mu}_i \qquad \text{Eq. A1}$$

with $\mathbf{L}$, $\mathbf{R}_i$, and μ_i given as,

$$\boldsymbol{\mu}_i = \left[x_{r_x} + \sum_{j=1}^{i-1} \cos(\theta_j)(l_j + u_{j+1}) \quad x_{r_y} + \sum_{j=1}^{i-1} \sin(\theta_j)(l_j + u_{j+1}) \quad 1 \quad u_i \quad u_{i+1} \right]^T,$$

$$\mathbf{L}^T = \begin{bmatrix} 1 & 0 & x & 0 & \frac{l-x}{l} & 0 & \frac{x}{l} & 0 \\ 0 & 1 & 0 & x & 0 & \frac{l-x}{l} & 0 & \frac{x}{l} \end{bmatrix} \mathbf{R}_i = \begin{bmatrix} 1 & 0 & 0 & 0 & 0 \\ 0 & 1 & 0 & 0 & 0 \\ 0 & 0 & c\theta_i & 0 & 0 \\ 0 & 0 & s\theta_i & 0 & 0 \\ 0 & 0 & 0 & c\theta_i & 0 \\ 0 & 0 & 0 & s\theta_i & 0 \\ 0 & 0 & 0 & 0 & c\theta_i \\ 0 & 0 & 0 & 0 & s\theta_i \end{bmatrix} \qquad \text{Eq. A2}$$

,

with $s\theta_i$, $c\theta_i = \sin(\theta_i)$, $\cos(\theta_i)$ respectively. Similarly, the particle velocity will be cast in the general form,

$$\dot{\mathbf{x}}_{pi} = \mathbf{L}^T \mathbf{R}'_i \, \dot{\boldsymbol{\mu}}'_i \qquad \text{Eq. A3}$$

with

$$\dot{\boldsymbol{\mu}}'_i = \left[\dot{x}_{r_x} + \sum_{j=1}^{i-1} \left[-\dot{\theta}_j \sin(\theta_j)(l_j + u_{j+1}) + \cos(\theta_j)\dot{u}_{j+1} \right] \quad \dot{x}_{r_y} + \sum_{j=1}^{i-1} \left[\dot{\theta}_j \cos(\theta_j)(l_j + u_{j+1}) + \sin(\theta_j)\dot{u}_{j+1} \right] \quad \dot{\theta}_i \quad \dot{\theta}_i u_i \quad \dot{\theta}_i u_{i+1} \quad \dot{u}_i \quad \dot{u}_{i+1} \right]$$

$$\mathbf{L}^T = \begin{bmatrix} 1 & 0 & x & 0 & L_1 & 0 & L_2 & 0 \\ 0 & 1 & 0 & x & 0 & L_1 & 0 & L_2 \end{bmatrix}, \mathbf{R}_i' = \begin{bmatrix} 1 & 0 & 0 & 0 & 0 & 0 & 0 \\ 0 & 1 & 0 & 0 & 0 & 0 & 0 \\ 0 & 0 & s\theta_i & 0 & 0 & 0 & 0 \\ 0 & 0 & c\theta_i & 0 & 0 & 0 & 0 \\ 0 & 0 & 0 & -s\theta_i & 0 & c\theta_i & 0 \\ 0 & 0 & 0 & c\theta_i & 0 & s\theta_i & 0 \\ 0 & 0 & 0 & 0 & -s\theta_i & 0 & c\theta_i \\ 0 & 0 & 0 & 0 & c\theta_i & 0 & s\theta_i \end{bmatrix} \quad \text{Eq. A4}$$

Based on Eqs. 14 and 17, the local mass and stiffness matrices for each element are given as,

$$\mathbf{m}_e = \rho A \begin{bmatrix} l & 0 & \frac{1}{2}l^2 & 0 & \frac{1}{2}l & 0 & \frac{1}{2}l & 0 \\ 0 & l & 0 & \frac{1}{2}l^2 & 0 & \frac{1}{2}l & 0 & \frac{1}{2}l \\ \frac{1}{2}l^2 & 0 & \frac{1}{3}l^3 & 0 & \frac{1}{6}l^2 & 0 & \frac{1}{3}l^2 & 0 \\ 0 & \frac{1}{2}l^2 & 0 & \frac{1}{3}l^3 & 0 & \frac{1}{6}l^2 & 0 & \frac{1}{3}l^2 \\ \frac{1}{2}l & 0 & \frac{1}{6}l^2 & 0 & \frac{1}{3}l & 0 & \frac{1}{6}l & 0 \\ 0 & \frac{1}{2}l & 0 & \frac{1}{6}l^2 & 0 & \frac{1}{3}l & 0 & \frac{1}{6}l \\ \frac{1}{2}l & 0 & \frac{1}{3}l^2 & 0 & \frac{1}{6}l & 0 & \frac{1}{3}l & 0 \\ 0 & \frac{1}{2}l & 0 & \frac{1}{3}l^2 & 0 & \frac{1}{6}l & 0 & \frac{1}{3}l \end{bmatrix} \quad \text{Eq. A5}$$

$$\mathbf{k}_e = \begin{bmatrix} 0 & 0 & 0 & 0 & 0 & 0 & 0 & 0 \\ 0 & 0 & 0 & 0 & 0 & 0 & 0 & 0 \\ 0 & 0 & lAE & 0 & -AE & 0 & AE & 0 \\ 0 & 0 & 0 & lAE & 0 & -AE & 0 & AE \\ 0 & 0 & -AE & 0 & \frac{AE}{l} & 0 & \frac{-AE}{l} & 0 \\ 0 & 0 & 0 & -AE & 0 & \frac{AE}{l} & 0 & \frac{-AE}{l} \\ 0 & 0 & AE & 0 & \frac{-AE}{l} & 0 & \frac{AE}{l} & 0 \\ 0 & 0 & 0 & AE & 0 & \frac{-AE}{l} & 0 & \frac{AE}{l} \end{bmatrix} \quad \text{Eq. A6}$$

and the local force vector is given as,

$$\mathbf{F}_e = \begin{bmatrix} f_x & f_y & \frac{1}{2}f_x l & \frac{1}{2}f_y l & \frac{1}{2}f_x l & \frac{1}{2}f_y l & \frac{1}{2}f_x l & \frac{1}{2}f_y l \end{bmatrix}. \quad \text{Eq. A5}$$

with f_x, f_y the force components acting on element i.

The elemental mass, stiffness matrices and velocity product matrices, $\mathbf{M}_{ei}$, $\mathbf{K}_{ei}$, $\mathbf{D}_{ei}$ resulting from the components of Lagranges equations given in Eqs. 20-23 are found as,

$$\mathbf{M}_{ei} = \begin{bmatrix} \partial\dot{\boldsymbol{\mu}}'^{T}_i/\partial\dot{q}_1 \\ \partial\dot{\boldsymbol{\mu}}'^{T}_i/\partial\dot{q}_2 \\ \vdots \\ \partial\dot{\boldsymbol{\mu}}'^{T}_i/\partial\dot{q}_m \end{bmatrix} \mathbf{R}'^{T}_i \, \mathbf{m}_e \mathbf{R}'_i \quad \mathbf{D}_{ei} = \left(\begin{bmatrix} \frac{d}{dt}\left(\partial\dot{\boldsymbol{\mu}}'^{T}_i/\partial\dot{q}_1\right) - \partial\dot{\boldsymbol{\mu}}'^{T}_i/\partial q_1 \\ \frac{d}{dt}\left(\partial\dot{\boldsymbol{\mu}}'^{T}_i/\partial\dot{q}_2\right) - \partial\dot{\boldsymbol{\mu}}'^{T}_i/\partial q_2 \\ \vdots \\ \frac{d}{dt}\left(\partial\dot{\boldsymbol{\mu}}'^{T}_i/\partial\dot{q}_m\right) - \partial\dot{\boldsymbol{\mu}}'^{T}_i/\partial q_m \end{bmatrix} \mathbf{R}'^{T}_i + 2\begin{bmatrix} \partial\dot{\boldsymbol{\mu}}'^{T}_i/\partial\dot{q}_1 \\ \partial\dot{\boldsymbol{\mu}}'^{T}_i/\partial\dot{q}_2 \\ \vdots \\ \partial\dot{\boldsymbol{\mu}}'^{T}_i/\partial\dot{q}_m \end{bmatrix} \dot{\mathbf{R}}'^{T}_i - \begin{bmatrix} \dot{\boldsymbol{\mu}}'^{T}_i \partial\mathbf{R}'^{T}_i/\partial q_1 \\ \dot{\boldsymbol{\mu}}'^{T}_i \partial\mathbf{R}'^{T}_i/\partial q_2 \\ \vdots \\ \dot{\boldsymbol{\mu}}'^{T}_i \partial\mathbf{R}'^{T}_i/\partial q_m \end{bmatrix} \right) \mathbf{m}_{ei} \mathbf{R}'_i$$

$$\mathbf{K}_{ei} = \left(\begin{bmatrix} \partial\boldsymbol{\mu}^{T}_i/\partial q_1 \\ \partial\boldsymbol{\mu}^{T}_i/\partial q_2 \\ \vdots \\ \partial\boldsymbol{\mu}^{T}_i/\partial q_m \end{bmatrix} \mathbf{R}^{T}_i + \begin{bmatrix} \boldsymbol{\mu}^{T}_i \partial\mathbf{R}^{T}_i/\partial q_1 \\ \boldsymbol{\mu}^{T}_i \partial\mathbf{R}^{T}_i/\partial q_2 \\ \vdots \\ \boldsymbol{\mu}^{T}_i \partial\mathbf{R}^{T}_i/\partial q_m \end{bmatrix} \right) \mathbf{k}_{ei} \mathbf{R}_i \qquad \text{Eq. A6}$$

while the elemental generalized force vector is,

$$\mathbf{Q}_{ei} = \begin{bmatrix} \mathbf{F}_{ei}\left(\mathbf{R}_i \, \partial\boldsymbol{\mu}_i/\partial q_1 + \partial\mathbf{R}_i/\partial q_1 \, \boldsymbol{\mu}_i\right) \\ \mathbf{F}_{ei}\left(\mathbf{R}_i \, \partial\boldsymbol{\mu}_i/\partial q_2 + \partial\mathbf{R}_i/\partial q_2 \, \boldsymbol{\mu}_i\right) \\ \vdots \\ \mathbf{F}_{ei}\left(\mathbf{R}_i \, \partial\boldsymbol{\mu}_i/\partial q_n + \partial\mathbf{R}_i/\partial q_n \, \boldsymbol{\mu}_i\right) \end{bmatrix}. \qquad \text{Eq. A7}$$

The system mass, stiffness and velocity product matrices are formed as combinations of the elemental matrices in the fashion demonstrated in the following equations. These matrices contain the coefficients of the generalized coordinate vector and its derivatives in the form $q = \lfloor x_{rx} \quad x_{ry} \quad \theta_1 \quad u_1 \quad u_2 \quad \theta_2 \quad u_3 \quad \cdots \rfloor$.

The global mass matrix, **M** is generated as,

$$
\begin{aligned}
\mathbf{M}(:,1) &= \sum_{i=1}^{n} \mathbf{M}_{ei}(:,1) \\
\mathbf{M}(:,2) &= \sum_{i=1}^{n} \mathbf{M}_{ei}(:,2) \\
\mathbf{M}(:,3) &= \mathbf{M}_{e1}(:,3) + u_1 \mathbf{M}_{e1}(:,4) + u_2 \mathbf{M}_{e1}(:,5) + \sum_{i=2}^{n} (l_1 + u_2)(-s_1 \mathbf{M}_{ei}(:,1) + c_1 \mathbf{M}_{ei}(:,2)) \\
\mathbf{M}(:,4) &= \mathbf{M}_{e1}(:,6) \\
\mathbf{M}(:,5) &= \mathbf{M}_{e1}(:,7) + \mathbf{M}_{e2}(:,6) + \sum_{i=2}^{n} (c_i \mathbf{M}_{ei}(:,1) + s_i \mathbf{M}_{ei}(:,2)) \\
\mathbf{M}(:,6) &= \mathbf{M}_{e2}(:,3) + u_2 \mathbf{M}_{e2}(:,4) + u_3 \mathbf{M}_{e2}(:,5) + \sum_{i=3}^{n} (l_2 + u_3)(-s_2 \mathbf{M}_{ei}(:,1) + c_2 \mathbf{M}_{ei}(:,2)) \\
&\vdots
\end{aligned}
\qquad \text{Eq. A8}
$$

The global velocity product matrix **D** is generated in a similar form as,

$$
\begin{aligned}
\mathbf{D}(:,1) &= \sum_{i=1}^{n} \mathbf{D}_{ei}(:,1) \\
\mathbf{D}(:,2) &= \sum_{i=1}^{n} \mathbf{D}_{ei}(:,2) \\
\mathbf{D}(:,3) &= \mathbf{D}_{e1}(:,3) + u_1 \mathbf{D}_{e1}(:,4) + u_2 \mathbf{D}_{e1}(:,5) + \sum_{i=2}^{n} (l_1 + u_2)(s_1 \mathbf{D}_{ei}(:,1) + c_1 \mathbf{D}_{ei}(:,2)) \\
&\quad + \sum_{i=2}^{n} \left(\mathbf{M}_{ei}(:,1)(-\dot{\theta}_1 c_1 (l_1 + u_2) - 2\dot{u}_2 s_1) + \mathbf{M}_{ei}(:,2)(-\dot{\theta}_{21} s_1 (l_1 + u_2) + 2\dot{u}_2 c_1) \right) \\
&\quad + \dot{u}_1 \mathbf{M}_{e1}(:,4) + \dot{u}_2 \mathbf{M}_{e1}(:,5) \\
\mathbf{D}(:,4) &= \mathbf{D}_{e1}(:,6) \\
\mathbf{D}(:,5) &= \mathbf{D}_{e1}(:,7) + \mathbf{D}_{e2}(:,6) + \sum_{i=2}^{n} (c_i \mathbf{D}_{ei}(:,1) + s_i \mathbf{D}_{ei}(:,2)) \\
\mathbf{D}(:,6) &= \mathbf{D}_{e2}(:,3) + u_2 \mathbf{D}_{e2}(:,4) + u_3 \mathbf{D}_{e2}(:,5) + \sum_{i=3}^{n} (l_2 + u_3)(s_2 \mathbf{D}_{ei}(:,1) + c_2 \mathbf{D}_{ei}(:,2)) \\
&\quad + \sum_{i=3}^{n} \left(\mathbf{M}_{ei}(:,1)(-\dot{\theta}_2 c_2 (l_2 + u_3) - 2\dot{u}_3 s_2) + \mathbf{M}_{ei}(:,2)(-\dot{\theta}_2 s_2 (l_2 + u_3) + 2\dot{u}_3 c_2) \right) \\
&\quad + \dot{u}_2 \mathbf{M}_{e2}(:,4) + \dot{u}_3 \mathbf{M}_{e2}(:,5) \\
&\vdots
\end{aligned}
\qquad \text{Eq. A9}
$$

The global stiffness matrix, **K** is generated as,

$$\begin{aligned}
&\mathbf{K}(:,1) = \sum_{i=1}^{n} \mathbf{K}_{ei}(:,1) \\
&\mathbf{K}(:,2) = \sum_{i=1}^{n} \mathbf{K}_{ei}(:,2) \\
&\mathbf{K}(:,3) = \mathbf{0} \\
&\mathbf{K}(:,4) = \mathbf{K}_{e1}(:,4) \\
&\mathbf{K}(:,5) = \mathbf{K}_{e1}(:,5) + \mathbf{K}_{e2}(:,4) + \sum_{i=2}^{n} \left(\mathbf{K}_{ei}(:,1)c_1 + \mathbf{K}_{ei}(:,2)s_1\right) \\
&\mathbf{K}(:,6) = \mathbf{0} \\
&\vdots
\end{aligned} \qquad \text{Eq. A10}$$

and the generalized vector of forces,

$$\mathbf{Q} = \sum_{i=1}^{n} \mathbf{Q}_{ei} = \sum_{i=1}^{n} \left(\begin{bmatrix} \mathbf{F}_{ei}\left(\mathbf{R}_i \, \partial \boldsymbol{\mu}_i / \partial q_1 + \partial \mathbf{R}_i / \partial q_1 \, \boldsymbol{\mu}_i \right) \\ \mathbf{F}_{ei}\left(\mathbf{R}_i \, \partial \boldsymbol{\mu}_i / \partial q_2 + \partial \mathbf{R}_i / \partial q_2 \, \boldsymbol{\mu}_i \right) \\ \vdots \\ \mathbf{F}_{ei}\left(\mathbf{R}_i \, \partial \boldsymbol{\mu}_i / \partial q_n + \partial \mathbf{R}_i / \partial q_n \, \boldsymbol{\mu}_i \right) \end{bmatrix} \right). \qquad \text{Eq. A11}$$

The system mass, stiffness and velocity product matrices and the total generalized force vector are developed as an example for a simple two-element system. This system has three nodes, two elements, and seven generalized coordinates. The results of this expansion are given in the following equations.

M: Eq. A12

$$\begin{aligned}
\mathbf{M}(1,:) &= \left[2l\rho \quad 0 \quad \tfrac{-1}{2}s_1 l\rho(l + u_1 + 3u_2) \quad \tfrac{1}{2}c_1 l\rho \quad \tfrac{-1}{2}l\rho(c_1 + 3c_2) \quad \tfrac{-1}{2}s_2 l\rho(-l + u_2 + u_3) \quad \tfrac{1}{2}c_2 l\rho\right] \\
\mathbf{M}(2,:) &= \left[0 \quad 2l\rho \quad \tfrac{1}{2}c_1 l\rho(3l + u_1 + 3u_2) \quad \tfrac{1}{2}s_1 l\rho \quad \tfrac{1}{2}l\rho(s_1 + 3s_2) \quad \tfrac{1}{2}c_2 l\rho(l + u_2 + u_3) \quad \tfrac{1}{2}s_2 l\rho\right] \\
\mathbf{M}(3,:) &= \left[\tfrac{-1}{2}s_1 l\rho(l + u_1 + 3u_2) \quad \tfrac{1}{2}c_1 l\rho(3l + u_1 + 3u_2) \quad m_{33} \quad \tfrac{1}{3}c_1 l^2 \rho s_1 \quad m_{35} \quad m_{36} \quad m_{37}\right] \\
\mathbf{M}(4,:) &= \left[\tfrac{1}{2}c_1 l\rho \quad \tfrac{1}{2}s_1 l\rho \quad \tfrac{1}{3}c_1 s_1 l^2 \rho \quad \tfrac{1}{3}l\rho \quad \tfrac{1}{6}l\rho \quad 0 \quad 0\right]
\end{aligned}$$

$$\mathbf{M}(5,:)=\left[\tfrac{1}{2}l\rho(3c_1+c_2)\quad \tfrac{1}{2}l\rho(3s_1+s_2)\quad m_{53}\quad \tfrac{1}{6}l\rho\quad \tfrac{1}{6}l\rho(7+9c_1c_2+9s_1s_2)\quad m_{56}\quad \tfrac{1}{6}l\rho(7+3c_1c_2+3s_1s_2)\right]$$
$$\mathbf{M}(6,:)=\left[-\tfrac{1}{2}s_2l\rho(-l+u_2+u_3)\quad \tfrac{1}{2}c_2l\rho(l+u_2+u_3)\quad m_{63}\quad 0\quad \tfrac{4}{3}c_2s_2l^2\rho\quad m_{66}\quad \tfrac{2}{3}c_2s_2l^2\rho\right]$$
$$\mathbf{M}(7,:)=\left[\tfrac{1}{2}c_2l\rho\quad \tfrac{1}{2}s_2l\rho\quad \tfrac{1}{2}(l+u_2)l\rho(-s_1c_2+c_1s_2)\quad 0\quad \tfrac{2}{3}l\rho\quad \tfrac{2}{3}c_2s_2l^2\rho\quad \tfrac{1}{3}l\rho\right]$$

with,

$$m_{33}=\tfrac{1}{3}l\rho\left(4l^2-lu_1+2lu_1c_1^2+4lu_2+4lu_2c_1^2+u_1^2+u_1u_2+4u_2^2\right)$$
$$m_{35}=\tfrac{1}{6}l\rho\left(4c_1ls_1-9s_1lc_2-9s_1u_2c_2+9c_1ls_2+9c_1u_2s_2\right)$$
$$m_{36}=\tfrac{1}{2}(l+u_2)l\rho\left(-s_1s_2l+s_1s_2u_2+s_1s_2u_3+c_1c_2l+c_1c_2u_2+c_1c_2u_3\right)$$
$$m_{37}=\tfrac{1}{2}(l+u_2)l\rho\left(-s_1c_2+c_1s_2\right)$$
$$m_{53}=\tfrac{1}{6}l\rho\left(4c_1s_1l-3s_1c_2l+3c_1s_2l-3s_1c_2u_2+3c_1s_2u_2\right)$$
$$m_{56}=\tfrac{1}{6}l\rho\left(-3c_1s_2l-2s_2c_2l-3s_1c_2l+3c_1s_2u_2-3s_1c_2u_2+3c_1s_2u_3-3s_1c_2u_3\right)$$
$$m_{63}=\tfrac{1}{2}(l+u_2)l\rho\left(-s_1s_2l+s_1s_2u_2+s_1s_2u_3+c_1c_2l+c_1c_2u_2+c_1c_2u_3\right)$$
$$m_{66}=\tfrac{1}{3}l\rho\left(l^2-lu_2+2c_2^2lu_2-2lu_3+4c_2^2lu_3+u_2^2+u_2u_3+u_3^2\right)$$

D: Eq. A13

$$\mathbf{D}(1,:)=\left[0\quad 0\quad \tfrac{-1}{2}l\rho\left(2\dot\theta_1c_1l+2\dot\theta_1u_2c_1+5\dot u_2s_1+\dot u_1s_1\right)\quad 0\quad 0\quad \tfrac{-1}{2}l\rho s_2(2\dot u_2+\dot u_3)\quad 0\right]$$
$$\mathbf{D}(2,:)=\left[0\quad 0\quad \tfrac{-1}{2}l\rho\left(2\dot\theta_1s_1l+2\dot\theta_1u_2s_1-5\dot u_2c_1-\dot u_1c_1\right)\quad 0\quad 0\quad \tfrac{1}{2}l\rho c_2(\dot u_2+\dot u_3)\quad 0\right]$$
$$\mathbf{D}(3,:)=\left[\tfrac{1}{2}\dot\theta l_1c_1l\rho(l-u_1-u_2)\quad \tfrac{1}{2}\dot\theta l_1s_1l\rho(l+u_1+u_2)\quad d_{33}\quad d_{34}\quad d_{35}\quad d_{36}\quad 0\right]$$
$$\mathbf{D}(4,:)=\left[\tfrac{-1}{2}l\rho\dot\theta_1s_1\quad \tfrac{1}{2}l\rho\dot\theta_1c_1\quad \tfrac{1}{6}l\rho\dot\theta_1\left(-l+2lc_1^2+2u_1+u_2\right)\quad 0\quad 0\quad 0\quad 0\right]$$
$$\mathbf{D}(5,:)=\left[\tfrac{-1}{2}l\rho\left(\dot\theta_1s_1+\dot\theta_2s_2\right)\quad \tfrac{1}{2}l\rho\left(\dot\theta_1c_1+\dot\theta_2c_2\right)\quad d_{53}\quad 0\quad 0\quad d_{56}\quad 0\right]$$
$$\mathbf{D}(6,:)=\left[\tfrac{-1}{2}\dot\theta_2c_2l\rho(-l+u_2+u_3)\quad \tfrac{-1}{2}\dot\theta_2s_2l\rho(l+u_2+u_3)\quad d_{63}\quad 0\quad d_{65}\quad d_{66}\quad d_{67}\right]$$
$$\mathbf{D}(7,:)=\left[\tfrac{-1}{2}\dot\theta_2s_2l\rho\quad \tfrac{1}{2}\dot\theta_2c_2l\rho\quad d_{7,3}\quad 0\quad 0\quad \tfrac{1}{3}\dot\theta_2l^2\rho\left(-1+2c_2^2\right)+\tfrac{1}{6}\dot\theta_2l\rho(u_2+2u_3)\quad 0\right]$$

with,

$$d_{33}=\tfrac{-1}{6}l\rho\left(4u_1\dot\theta_1s_1+8\dot\theta_1u_2s_1c_1l-10\dot u_2l-4c_1^2l\dot u_2-14\dot u_2u_2+\dot u_1l-2\dot u_1lc_1^2-2\dot u_1u_1-\dot u_1u_2-\dot u_2u_1\right)$$
$$d_{34}=\tfrac{1}{6}\dot\theta l_1l\rho\left(2c_1^2l-l-2u_1-u_2\right)$$
$$d_{35}=\tfrac{1}{6}\dot\theta l_1l\rho\left(4c_1^2l-2l-u_1-2u_2\right)$$
$$d_{36}=\tfrac{1}{2}l\rho\left(4\dot u_2ls_1s_2+\dot u_2u_2s_1s_2+\dot u_2lc_1c_2+\dot u_2u_2c_1c_2+\dot u_3ls_1s_2+\dot u_3u_2s_1s_2\right)$$
$$d_{53}=\tfrac{-1}{6}l\rho\begin{pmatrix}-4l\dot\theta_1c_1^2+8\dot\theta_1l-u_1\dot\theta_1+4\dot\theta_1u_2+3s_1s_2\dot\theta_2l-3c_1c_2\dot\theta_2l+3s_1s_2\dot\theta_2u_2-3c_1c_2\dot\theta_2u_2\\+3c_1c_2\dot\theta_1l+3c_1c_2\dot\theta_1u_2+6s_1c_2\dot u_2+3s_1s_2\dot\theta_1l+3s_1s_2\dot\theta_1u_2-6c_1s_2\dot u_2\end{pmatrix}$$

$$d_{56} = \tfrac{1}{6} l\rho\left(\dot{\theta}_2 l + 2\dot{\theta}_2 l c_2^2 + 2u_2\dot{\theta}_2 + u_3\dot{\theta}_2 - 3\dot{u}_2 s_1 c_2 + 3\dot{u}_2 s_1 c_2 - 3\dot{u}_3 c_1 s_2 + 3\dot{u}_3 s_1 c_2\right)$$

$$d_{63} = \left(l + u_2\right)\left(-\frac{1}{2} s_1 c_2 \dot{\theta}_2 l\rho\left(-l + u_2 + u_3\right) - \frac{1}{2} c_1 s_2 \dot{\theta}_2 l\rho\left(l + u_2 + u_3\right)\right) - \frac{1}{2} s_2 l\rho\left(-l + u_2 + u_3\right)$$
$$\left(-\dot{\theta}_1 c_1\left(l + u_2\right) + 2\dot{u}_2 s_1\right) + \frac{1}{2} c_2 l\rho\left(l + u_2 + u_3\right)\left(-\dot{\theta}_1 s_1\left(l + u_2\right) + 2\dot{u}_2 c_1\right)$$

$$d_{65} = -\tfrac{1}{6}\dot{\theta}_2 l\rho\left(-2c_2^2 l + l + 2u_2 + u_3\right) - \tfrac{1}{2} c_2^2 \dot{\theta}_2 l\rho\left(-l + u_2 + u_3\right) - \tfrac{1}{2} s_2^2 \dot{\theta}_2 l\rho\left(l + u_2 + u_3\right)$$

$$d_{66} = -\tfrac{1}{3} s_2 c_2 \dot{\theta}_2 l^2 \rho\left(2u_2 + 4u_3\right) + \tfrac{1}{6}\dot{u}_2 l\rho\left(-l + 2c_2^2 l + 2u_2 + u_3\right) + \tfrac{1}{6}\dot{u}_3 l\rho\left(-2l + 4c_2^2 l + 2_2 + 2u_3\right)$$

$$d_{67=} \tfrac{-1}{6}\dot{\theta}_2 l\rho\left(-4lc_2^2 + 2l + u_2 + 2u_3\right)$$

$$d_{73} = \left(l + u_2\right)\left(\tfrac{-1}{2}\dot{\theta}_2 s_1 s_2 l\rho + \tfrac{1}{2}\dot{\theta}_2 c_1 c_2 l\rho\right) + \tfrac{1}{2} c_2 l\rho\left(-\dot{\theta}_2 c_1\left(l + u_2\right) + 2\dot{u}_2 c_1\right)$$

K:

$$\mathbf{K} = \begin{bmatrix} 0 & 0 & 0 & 0 & 0 & 0 & 0 \\ 0 & 0 & 0 & 0 & 0 & 0 & 0 \\ 0 & 0 & 0 & 0 & 0 & 0 & 0 \\ 0 & 0 & 0 & \dfrac{AE}{l} & \dfrac{-AE}{l} & 0 & 0 \\ 0 & 0 & 0 & \dfrac{-AE}{l} & \dfrac{2AE}{l} & 0 & \dfrac{-AE}{l} \\ 0 & 0 & 0 & 0 & 0 & 0 & 0 \\ 0 & 0 & 0 & 0 & \dfrac{-AE}{l} & 0 & \dfrac{AE}{l} \end{bmatrix} \qquad \text{Eq. A14}$$

Q:

$$\mathbf{Q} = \begin{bmatrix} f_{x1} + f_{x2} \\ f_{y1} + f_{y2} \\ \begin{bmatrix} \frac{1}{2}\left(-f_{x1} s_1 + f_{y1} c_1\right)\left(l + u_1 + u_2\right) \\ \left(-f_{x2} s_1 + f_{y2} c_1\right)\left(l + u_2\right) \end{bmatrix} \\ \begin{bmatrix} \frac{1}{2}\left(f_{x1} s_1 + f_{y1} c_1 + f_{x2} s_2 + f_{y2} c_2\right) \\ + f_{x2} s_1 + f_{y2} c_1 \end{bmatrix} \\ \frac{1}{2}\left(-f_{x1} s_1 + f_{y1} c_1\right) \\ \frac{1}{2}\left(-f_{x2} s_2 + f_{y2} c_2\right)\left(l + u_2 + u_3\right) \\ \frac{1}{2}\left(f_{x2} c_2 + f_{y2} s_2\right) \end{bmatrix} \qquad \text{Eq. A15}$$

Dynamics of a flexible, flying tether:

The dynamics of a flexible tether are evaluated through a continuous cable system model undergoing axial vibration. This continuous system model considers longitudinal vibration before, during and after a capture episode, and during and after a release episode. The model system equations are derived from Fig. 1 as follows.

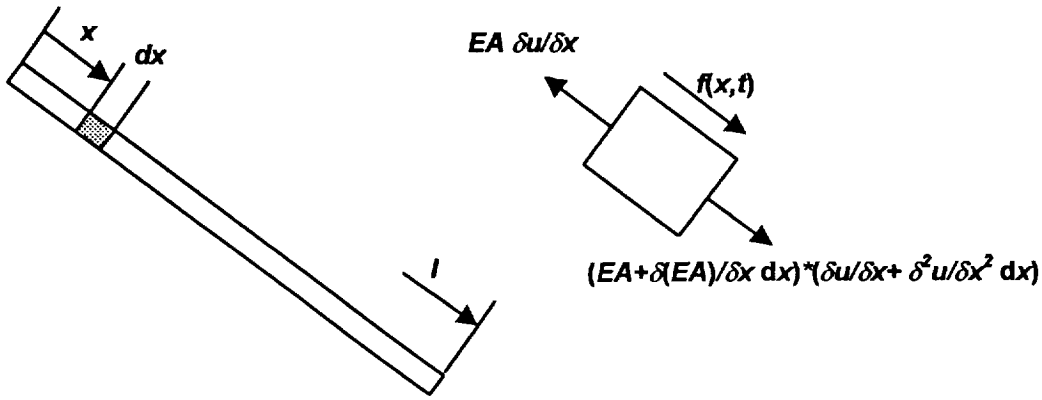

Fig. 1: Cable diagram and free body

The force balance for a small element of cable, dx is given as,

$$-EA\,\partial u/\partial x + \left(EA + \partial EA/\partial x\,dx\right)\left(\partial u/\partial x + \partial^2 u/\partial x^2\,dx\right) + f(x,t)dx = \rho\frac{\partial^2\left(\mathbf{x}_r + x_{el} + u\right)}{\partial t^2}dx \quad \text{Eq. 1}$$

with $u = u(x,t)$ the tether displacement at location x and time t, E, A, and ρ the cable modulus, area and mass per unit length. Assuming uniform tether properties and dividing through by dx yields,

$$f(x,t) = \rho\frac{\partial^2\left(\mathbf{x}_r + x_{el} + u\right)}{\partial t^2} + EA\,\partial^2 u/\partial x^2 \quad \text{Eq. 2}$$

This displacement function represents the flexible-body motion of the tether, while xr and xel are rigid body position vectors representing rigid body motion of the tether. $f(x,t)$ represents the forces per unit length acting on the tether.

Next, a solution to the flexible tether dispacement function, $u(x,t)$ is constructed as a sum of mode shapes and time dependent generalized coordinates,

$$\mathbf{u}(x,t) = \sum_{r=1}^{\infty} U_r(x)q_r(t)\hat{u}\,. \quad \text{Eq. 3}$$

with $U_r(x)$ representing the modes shapes of the tether. These mode shapes are derived as solutions to the spatial differential equation,

$$d^2U(x)/dx^2 + \frac{\omega^2\rho}{EA}U(x) = 0 \quad \text{Eq. 4}$$

as,

$$U(x) = C_1\sin(\beta x) + C_2\cos(\beta x) \quad \text{Eq. 5}$$

with $\beta = \frac{\omega^2 \rho}{EA}$. Coefficients C_1 and C_2 are determined from the boundary conditions to the problem. For the free-flying MXER tether, consider the homogenous boundary conditions associated with free-free tether ends. These are described as,

$$EA \partial u(0,t)/\partial x = 0$$
$$EA \partial u(l,t)/\partial x = 0 \qquad \text{Eq. 6}$$

Solving Eq. 5 for coefficients C_1 and C_2 yields the following mode shape vector and natural frequencies,

$$U_r(x) = B_r \cos\left(\frac{r\pi x}{l}\right) \qquad \text{Eq. 7}$$

$$\omega_r = r\pi \sqrt{\frac{EA}{\rho l^2}} \qquad \text{Eq. 8}$$

for $r = 0, 1, 2, \ldots$ with $r = 0$ representing the rigid body mode of the tether.
The modes in Eq. 7 are normalized resulting in the normal modes for the free-free tether as

$$U_r(x) = \sqrt{\frac{2}{\rho l}} \cos\left(\frac{r\pi x}{l}\right), r = 1, 2, \ldots \qquad \text{Eq. 9}$$

with the following normalizing functions employed,

$$\int_0^L \rho U_r(x) U_s(x) dx = \delta_{rs}, r,s = 1,2,\ldots \qquad \text{Eq. 10}$$

that also satisfy the function

$$\int_0^L U_s(x) EA \partial U_r(x)/\partial x dx = \omega_r^2 \delta_{rs}, r,s = 1,2,\ldots \qquad \text{Eq. 11}$$

With the mode shapes derived, the displacement solution form of Eq. 3 is substituted into Eq. 2 to result in,

$$m\ddot{\mathbf{x}}_r + m\boldsymbol{\alpha} \times \mathbf{x}_{el} + m\boldsymbol{\omega} \times \boldsymbol{\omega} \times \mathbf{x}_{el} + m\sum_{r=1}^{\infty} U_r(x)\ddot{q}_r(t)\hat{u} + m\boldsymbol{\alpha} \times \sum_{r=1}^{\infty} U_r(x) q_r(t)\hat{u} + m\boldsymbol{\omega} \times \boldsymbol{\omega} \times \sum_{r=1}^{\infty} U_r(x) q_r(t)\hat{u}$$
$$+ 2m\boldsymbol{\omega} \times \sum_{r=1}^{\infty} U_r(x)\dot{q}_r(t)\hat{u} + \sum_{r=1}^{\infty} q_r(t) EA \frac{d^2 U_r(x)}{dx^2}\hat{u} = \mathbf{f}(x,t) \qquad \text{Eq. 12}$$

or

$$m\sum_{r=1}^{\infty} U_r(x)\ddot{q}_r(t)\hat{u} + 2m\boldsymbol{\omega} \times \sum_{r=1}^{\infty} U_r(x)\dot{q}_r(t)\hat{u} + m(\boldsymbol{\alpha} \times + \boldsymbol{\omega} \times \boldsymbol{\omega} \times)\sum_{r=1}^{\infty} U_r(x) q_r(t)\hat{u}$$
$$+ \sum_{r=1}^{\infty} q_r(t) EA \frac{d^2 U_r(x)}{dx^2}\hat{u} = \mathbf{f}(x,t) - m(\ddot{\mathbf{x}}_r + \boldsymbol{\alpha} \times \mathbf{x}_{el} + \boldsymbol{\omega} \times \boldsymbol{\omega} \times \mathbf{x}_{el}) \qquad \text{Eq. 13}$$

with α, ω the rigid body rotation rates and accelerations, $\mathbf{x}_r$ a reference vector locating the tether (fig. 1) and $\mathbf{x}_{el}$ a vector running along the tether from the reference point to the location of the element of interest. Using the fact that the modes $U_r(x)$ have been normalized based on Eq. 10 and satisfy Eq. 11, Eq. 13 can be multiplied through by $U_r(x)$ and integrated over the tether length, L as,

$$\sum_{r=0}^{\infty}\int_0^L mU_s(x)U_r(x)\ddot{q}_r(t)dx\hat{u} + 2m\omega\times\sum_{r=1}^{\infty}\int_0^L mU_s(x)U_r(x)q_r(t)dx\hat{u} + \sum_{r=0}^{\infty}(\alpha\times+\omega\times\omega\times)\int_0^L mU_s(x)U_r(x)q_r(t)dx\hat{u}$$

$$+\sum_{r=0}^{\infty}\int_0^L U_s(x)EA\frac{d^2U_r(x)}{dx^2}q_r(t)dx\hat{u} = \int_0^L U_r(x)(\mathbf{f}(x,t) - m(\ddot{\mathbf{x}}_r + \alpha\times\mathbf{x}_{el} + \omega\times\omega\times\mathbf{x}_{el}))dx$$

Eq. 14

To yield the following set of differential equations,

$$\ddot{q}_r(t)\hat{u} + 2\omega\times\dot{q}_r(t)\hat{u} + +(\alpha\times+\omega\times\omega\times)q_r(t)\hat{u} + \omega_r q_r(t)\hat{u} = Q_r(t)\hat{Q}_r \qquad \text{Eq. 15}$$

This vector set of equations can be decomposed into axial and transverse components as,

$$\ddot{q}_r(t) + (-\dot{\theta}^2(t) + \omega_r)q_r(t) = Q_{r,axial}(t) \qquad \text{Eq. 16}$$

the axial components and

$$\dot{\theta}(t)\dot{q}_r(t) + \ddot{\theta}(t)q_r(t) = Q_{r,trans}(t) \qquad \text{Eq. 17}$$

with ω_r given in eq. 8, $\dot{\theta}(t), \ddot{\theta}(t)$ the scalar tether rotation rate and acceleration respectively, and $Q_{r,axial}(t), Q_{r,trans}(t)$ the axial and transverse external forces and rigid body inertial effects respectively with $Q_r(t)$ given as,

$$Q_r(t) = \int_0^L U_s(x)(f(x,t) - m(\ddot{\mathbf{x}}_r + \alpha\times\mathbf{x}_{el} + \omega\times\omega\times\mathbf{x}_{el}))dx \qquad \text{Eq. 19}$$

for $r = 0,1,2,\ldots$

The above equations, for example Eqs. 15 and 19 demonstrate the inherent coupling between the rigid body motion and the elastic response. The response of the rigid body tether is considered next.

Response of Rigid Body Tether:

The rigid body tether motion under the effects of a spherical gravity model is considered next. A uniform, rigid tether is assumed in a planar orbit, as shown in fig. 2.

Figure 2: Uniform rigid tether in planar orbit.

The energy of the system with respect to the generalized coordinates is given as,

$$T = \tfrac{1}{2}m_t v_{t,cm}^T \mathbf{v}_{t,cm} + \tfrac{1}{2}\dot{\phi}^2 I_t$$

$$V = \frac{-\mu m_t}{r_t} \qquad \text{Eq. 20}$$

with m_t, the tether mass, $\mathbf{I}_t$ the tether mass moment of inertia, $\mathbf{r}_t$, $\mathbf{v}_t$ and ϕ_t the position, velocity and angular rate of the tether center of mass,

$$\mathbf{r}_t = x_r e^{i\phi} + l/2\, e^{i\theta}$$
$$\mathbf{v}_t = \dot{x}_r e^{i\phi} + x_r i\dot{\phi} e^{i\phi} + l/2\, i\dot{\theta} e^{i\theta} \qquad \text{Eq. 21}$$

Lagrange's equations for the rigid body tether result as,

$$m_t \ddot{x}_r - m_t x_r \dot{\theta}^2 + \frac{\mu m_t \left(x_r + l/2 \cos(\theta - \phi)\right)}{\left(x_r^2 + l^2/4 + x_r l \cos(\theta - \phi)\right)^{3/2}} = 0 \qquad \text{Eq. 22}$$

$$m_t x_r^2 \ddot{\theta} + 2 m_t x_r \dot{x}_r \dot{\theta} + \frac{\mu m_t \left(-x_r l \sin(\theta - \phi)\right)}{\left(x_r^2 + l^2/4 + x_r l \cos(\theta - \phi)\right)^{3/2}} = 0 \qquad \text{Eq. 23}$$

$$\left(m_t l^2/4 + I_t\right)\ddot{\phi} + \frac{\mu m_t \left(x_r l \sin(\theta - \phi)\right)}{\left(x_r^2 + l^2/4 + x_r l \cos(\theta - \phi)\right)^{3/2}} = 0. \qquad \text{Eq. 24}$$

Equations 22-24 present the tether rigid body motion, while eqs. 3 and 16 give the elastic body displacements of the tether. A method of evaluating the total elastic behavior of the tether system is now considered.

Consider a tether system as depicted in figs. 1 and 2 starting with initial orbit and rotation conditions, $\mathbf{x}_r$=6000000e^{i0}, θ_0=0, thetadot0=.13, thetaddot0=0, First, the rigid body motion of the tether is evaluated, allowing the tether body angular rate to be observed. Equations 22-24 are evaluated over a period of time with solutions for x_r, θ and ϕ evaluated. Plots of q, $\dot{\theta}(t), \ddot{\theta}(t)$ are shown in fig. 3

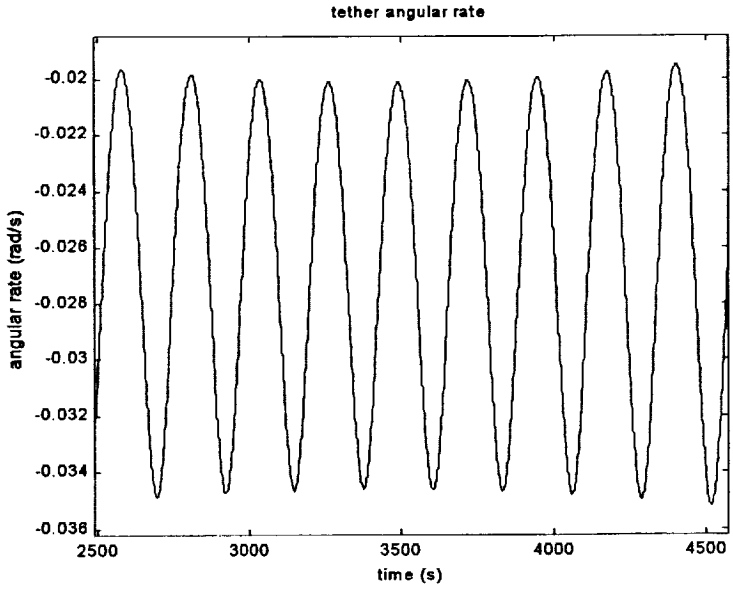

Fig. 3, plot of example rigid body tether angular rate under steady-state conditions

From fig. 3, the angular rate can be approximately described by the following sinusoidal function,

$$\dot{\theta}^2 = c_1 \cos(\omega t) + c_2 \qquad \text{Eq. 25}$$

or as a taylor series expansion

$$\dot{\theta}^2 = c_1 \sum \frac{(-1)^n}{(2n+1)!} t^{2n+1} + c_2 \qquad \text{Eq. 26}$$

with c_1=.0075, c_2=.00275 and w = pi/75.
The general elastic response for $u(x,t)$ for a set of initial conditions can now be presented. First, consider the solution for the generalized coordinates of Eq. 16. The homogenous solution to Eq. 16 is:

$$q_1 = a_0\left[1-\left(\frac{c_1+\omega_r}{2}\right)x^2+\frac{1}{24}\left(c_1\omega^2+(c_1+\omega_r)^2\right)x^4+\ldots\right]$$
$$q_2 = a_1\left[x-\left(\frac{c_1+\omega_r}{3}\right)x^3+\frac{1}{40}\left(c_1\omega^2+\frac{(c_1+\omega_r)^2}{3}\right)x^5+\ldots\right] \qquad \text{Eq. 27}$$

with the general solution of q given in the form

$$q_h = \sum_{n=0}^{\infty} a_n t^n \qquad \text{Eq. 28}$$

and a_0, a_1 coefficients determined from the initial value problem. Using these solutions for the homogenous problem and the method of variation of parameters, the particular solution for q is given as

$$q = -q_1(t)\int^t \frac{q_2(\tau)Q(\tau)}{q_1(\tau)q'_2(\tau)-q'_1(\tau)q_2(\tau)}d\tau + q_2(t)\int^t \frac{q_1(\tau)Q(\tau)}{q_1(\tau)q'_2(\tau)-q'_1(\tau)q_2(\tau)}d\tau. \qquad \text{Eq. 28}$$

Finally, the elastic displacement of the tether is given as,

$$u(x,t)=\sum_{r=1}^{\infty} U_r(x)\left[-q_1(t)\int^t \frac{q_2(\tau)Q(\tau)}{q_1(\tau)q'_2(\tau)-q'_1(\tau)q_2(\tau)}d\tau + q_2(t)\int^t \frac{q_1(\tau)Q(\tau)}{q_1(\tau)q'_2(\tau)-q'_1(\tau)q_2(\tau)}d\tau\right]_r \qquad \text{Eq. 29}$$

The solution for $u(x,t)$ depends on the generalized forcing function, Q_r. This depends on both the external forces on the tether and the rigid body tether motion. Consider the distributed force to be a constant gravitational load, fo and the rigid body motion given in the following section. Then, the generalized forces become,

$$Q_r(t) = \sqrt{\tfrac{2}{\rho L}}\left(f_o - m\ddot{x}_{ref}\right)\int_0^L \cos\left(\tfrac{r\pi x}{L}\right)dx - \sqrt{\tfrac{2}{\rho L}}m\left(\ddot{\theta}-\dot{\theta}^2\right)\int_0^L \cos\left(\tfrac{r\pi x}{L}\right)x\,dx,\ r = 0,1,\ldots \qquad \text{Eq. 19}$$

or

$$Q_r(t) = -2\sqrt{\tfrac{2}{\rho L}}m\left(\ddot{\theta}-\dot{\theta}^2\right)\frac{L^2}{r^2\pi^2},\ r = 1,3,\ldots \qquad \text{Eq. 20}$$

substituting the value of Qr back into eq. 17 yields,

$$u(x,t)=\sum_{r=1}^{\infty} U_r(x)\left[-q_1(t)\int^t \frac{q_2(\tau)-2\sqrt{\frac{2}{\rho L}}m\left(\ddot{\theta}-\dot{\theta}^2\right)\frac{L^2}{r^2\pi^2}}{q_1(\tau)q'_2(\tau)-q'_1(\tau)q_2(\tau)}d\tau + q_2(t)\int^t \frac{q_1(\tau)-2\sqrt{\frac{2}{\rho L}}m\left(\ddot{\theta}-\dot{\theta}^2\right)\frac{L^2}{r^2\pi^2}}{q_1(\tau)q'_2(\tau)-q'_1(\tau)q_2(\tau)}d\tau\right]_r$$

This equation can be expanded for the first relevant modes and evaluated